ELSEVIER

International Journal of Mass Spectrometry 214 (2002) 105–128

International Journal of Mass Spectrometry

www.elsevier.com/locate/ijms

Dissociation behavior of ionized valeramide Part I. Experimental studies

Jessica Loos [a], Detlef Schröder [a,*], Waltraud Zummack [a], Helmut Schwarz [a], Roland Thissen [b], Odile Dutuit [b]

[a] *Institut für Chemie der Technischen Universität Berlin, D-10623 Berlin, Germany*
[b] *Laboratoire de Chimie Physique, Bât. 350, Université Paris-Sud, 91405 Orsay, France*

Received 23 November 2001; accepted 3 December 2001

Abstract

The unimolecular dissociation of ionized valeramide (n-$C_4H_9CONH_2$) is examined by mass spectrometric techniques. Photoionization (PI) experiments yield an ionization energy of 9.40 ± 0.03 eV. Besides the formation of the molecular ion, dissociation is observed close to the onset of PI. In addition to the PI experiments, the unimolecular dissociations of metastable valeramide ions generated by electron ionization (EI) are examined by means of tandem mass spectrometry, including extensive deuterium labeling studies. The major dissociation processes correspond to competing losses of (i) neutral propene formed via the McLafferty rearrangement and (ii) an ethyl radical to presumably afford protonated acrylamide; losses of methyl radical as well as ethene occur as side reactions. The labeling studies reveal that the McLafferty reaction occurs with high specificity, whereas loss of an ethyl radical is associated with a pronounced, yet by no means complete hydrogen equilibration of the alkyl backbone. While most results of the dissociative PI experiments and the metastable ion (MI) studies agree quite well, significant variations of the ratios of C_3H_6 and $C_2H_5^\bullet$ losses in the various experiments do not find an immediate explanation and require further considerations. (Int J Mass Spectrom 214 (2002) 105–128)

Keywords: C–H bond activation; Coincidence spectra; Distonic ions; Mass spectrometry; Valeramide

1. Introduction

The McLafferty rearrangement [1,2] is arguably among the most important fragmentation processes in organic mass spectrometry [3]. Thus, ionized carbonyl compounds of sufficient chain length give rise to specific 1,5-hydrogen transfers followed by β-C–C bond cleavage affording an alkene and an enol. Which of the two fragments bears the positive charge depends on the relative ionization energies of the corresponding neutrals (Stevenson's rule). In many cases, the corresponding McLafferty fragments are rather abundant in the EI mass spectra, thereby providing valuable structural information for analytical purposes. A key aspect of the McLafferty rearrangement is its generality in that in addition to all kinds of carbonyl compounds, e.g., ketones, acids, esters, amides, and also aldehydes, numerous other compounds having multiple bonds give rise to variants of this characteristic fragmentation. Another notable feature of the McLafferty reaction is its high specificity even in cases where other fragmentation reactions—often associated with extensive skeletal rearrangements—compete efficiently. In some cases,

* Corresponding author. E-mail: df@www.chem.tu-berlin.de

1387-3806/02/$20.00
PII S1387-3806(01)00586-3

however, the McLafferty rearrangement seems to vanish in the metastable ion (MI) spectra of mass-selected metastable cation radicals of, for example, some carboxylic acids [4–7] and their derivatives [8,9].

Inspired by a paper of Kreft and Grützmacher [10] about unexpectedly large differences between the electron ionization (EI) and MI mass spectra of hexanoic acid and also its amide, we initiated a collaborative investigation of the dissociation behavior of ionized valeramide **1**, where specifically the EI, photoionization (PI), and MI mass spectra are compared. Amides were chosen because of the relevance of this class of compounds in biological chemistry, and the present examination of valeramide may further stimulate research on the gas phase ion chemistry of these and structurally related molecules. The specific choice of valeramide as a model system had the following reasons. (i) The alkyl chain of valeramide is just long enough to allow involvement of a secondary C–H bond in the McLafferty rearrangement; in addition, this substrate offers the opportunity to study stereochemical features, e.g., diastereoselective bond activation, by introducing further substituents [11]. (ii) In turn, the limited length of the backbone minimizes the number of possibly competing reactions. (iii) Likewise, the valeramide molecule is small enough to enable both extensive isotopic labeling of all positions of interest as well as adequate computational studies. (iv) Last but not least, some volatility criteria had to be met in the PI experiments, and the vapor pressure of valeramide is just at the borderline of practicability.

The experimental studies reported here (Part I) are complemented by two subsequent articles. Part II deals with a theoretical description of ionized valeramide and the various dissociation channels. Part III summarizes all results, explains the remaining discrepancies, and addresses the consequences for the interpretation of MI spectra of ionized carbonyl compounds.

2. Experimental methods

Most experiments were performed using a modified VG ZAB/HF/AMD 604 four-sector mass spectrometer of *BEBE* configuration (*B* stands for magnetic and *E* for electric sector) which has been described elsewhere [12]. In brief, the amides were introduced via a solid probe (no heating) and ionized by electrons with 70 eV kinetic energy at a repeller voltage of ca. 30 V. All ions were accelerated to 8 keV kinetic energy, those of interest mass-selected using *B*(1) and *E*(1), and the unimolecular dissociations of the molecular ion $\mathbf{1}^{+\bullet}$, its isotopologs or fragments in the field-free regions preceding *B*(2) were monitored by scanning this sector [13,14]. The spectra were accumulated and on-line processed with the AMD/Intectra data system; 8–20 scans were accumulated. The fragment ion intensities were derived from peak heights; consideration of peak areas, rather than heights, does not affect the branching ratios within the experimental error [11]. The data given in Table 1 were collected under strict EI conditions at a source temperature of 200 °C and are averaged over at least five independent measurements of each compound. Some additional experiments concerning the fragments of ionized valeramide were conducted under the conditions of chemical ionization (CI, repeller voltage ca. 0 V).

Valeramide forms a relatively weak molecular ion upon EI with several fragments of similar or even much larger abundances (see below). Particularly important for the analysis of the experimental data is that the molecular ion $M^{+\bullet}$ and the $[M-H]^+$ fragment are formed in similar amounts upon EI. As a consequence, the mass-selected $M^{+\bullet}$ ions are inherently interfered by ca. 5% of the $^{13}C_1$-isotopes of the $[M-H]^+$ fragment; the mass difference of 0.005 amu between $\mathbf{1}^{+\bullet}$ and the $^{13}C_1$-isotope of $[\mathbf{1}-H]^+$ (both $m/z = 101$) is too small to be resolved in MS/MS experiments with a sector instrument [13]. Mass-selected $[M-H]^+$ ions undergo two major unimolecular dissociations in a ca. 2:1 ratio, namely, losses of NH_3 and HNCO ($\Delta m = -17$ and -43, respectively) with the corresponding shifts upon labeling. In order to correct for this and other isobaric interferences, the MI spectra of the $[M-H]^+$ and $[M+H]^+$ species were recorded under identical source conditions with the same adjustments of the detector, amplifier, ion optics, etc. as used for $M^{+\bullet}$, thereby allowing to subtract the absolute fragment ion

Table 1
Mass differences (Δm in amu), normalized intensities[a,b,c], and branching ratios of C_1-, C_2-, and C_3-channels[d] observed in the corrected[e] MI spectra of $B(1)/E(1)$ mass-selected $\mathbf{1}^{+\bullet}$ and its isotopologs

	C_1[d]	−15	−17	−18	−19	C_2[d]	−28	−29	−30	−31	−32	−33	−34	C_3[d]	−42	−43	−44	−45	−46	−47
1	2	2	<1	<1		49	7	42						49	49	<1				
1a	2	2		<1	<1	49	7	42	<1					49	49	<1	1			
1b	2	2	<1	<1		45	7	7	12	19				53	53	<1				
1c	1	1	<1	<1		52	5	29	1	17				47	<1	7	40			
1d	3	2	<1	<1		50	<1	25	25					48	19	29	<1			
1e	2	2	<1	<1		53		21	7	25				45		37	8			
1f	3	<1	<1	2		41	<1		15	15	11			56		<1	8	48		
1g	3	<1	<1	2		42		<1	7	2	9	14	10	55		<1		<1	51	4

[a] Normalized to $\Sigma = 100$.
[b] The relative errors range from ca. ±5% for the most intense fragments to ±50% for the minor fragments.
[c] Numbers given as integers; rounding errors may occur. For a more complete compilation of the data, see Appendix A.
[d] The columns sum the separate channels as classified in the text ($\Sigma = 100$). Thus, C_1 comprises $\Delta m = -15$ to -19, C_2 comprises $\Delta m = -28$ to -34, C_3 comprises $\Delta m = -42$ to -47.
[e] The corrections mainly concern the channels $\Delta m = -17$ and -43 (with the respective shifts upon labeling) and involve a deconvolution of the interferences of the molecular ions by $^{13}C_1$-isotopes of the $[M - H]^+$ cations; for details, see Section 2.

signals after scaling for the ^{13}C abundancies and acknowledgment of the associated mass shifts. Because the correction procedure was adjusted to strictly avoid negative intensities, some remainder for the signals at $\Delta m = -17$ and -43 has to be accepted. Interferences by $[M+H]^+$, viz. incompletely deuterated, protonated amides, are negligible because (i) the samples had at least 94 at.% D, (ii) the amount of protonation is relatively low under EI conditions, and (iii) the protonated amides decay much more slowly (loss of ammonia prevails) than the cation radicals $M^{+\bullet}$. In fact, at least under EI conditions, the MI spectra of the mass-selected $[M + \mathbf{1}]^+$ peaks are governed by fragmentations due to the expected pattern of isobaric $^{13}C_1$-$M^{+\bullet}$.

PI studies of valeramide were performed in the CERISES apparatus [15] which was installed on the beam line SA63 of the synchrotron radiation source SuperACO at LURE (Orsay, France). This beam line is a normal incidence monochromator which provides tunable VUV-light in the range of 7–35 eV photon energy. Slits were at all time opened to 1 mm, corresponding to a photon energy resolution in the range of 500 (e.g., 20 meV at 10 eV). The accuracy of the photon energy was verified by measuring the ionization energy of argon within 2 meV of its nominal value. Below 11.8 eV, higher-order light from the grating of the monochromator was removed by means of a lithium fluoride window. The ions formed were extracted by a small electrostatic field (1 V/cm) towards an octopole ion guide and then a quadruple mass spectrometer (Nermag 350 mm), where mass selection was performed. Detection was achieved by means of multichannel plates operated in the counting mode. Spatially opposite to the cation detection system, photoelectron (PE) can be analyzed in an angularly discriminating time-of-flight spectrometer so that only threshold electrons are likely to be detected. Coupled operation of PE and photoion detectors with time-structured synchrotron radiation allows for coincidence measurements with threshold photoelectron-photoion coincidence (TPEPICO) [16]. The PI experiments further included appearance energy measurements in single-ion monitoring mode and mass spectra at different photon energies. The ion intensities were determined from peak heights and afterwards corrected for the natural abundance of ^{13}C. In the course of the experiments, CERISES has been upgraded to MS/MS capabilities by implementing a quadruple/octopole/quadruple arrangement. Therefore, recently also MI studies became feasible (see Part III).

Valeramide was introduced into CERISES by connecting a small vial containing a few mg of the sample directly to the source cell via a 50 cm long stainless steel tube. Unfortunately, but not entirely unexpected, a polar compound such as valeramide shows a substantial memory effect in that overnight pumping does not completely remove the residual amide adsorbed on the surfaces of the high-vacuum device (10^{-7} mbar). Moreover, some of the amide cannot be removed from the surface by pumping alone, and is only liberated when another amide (or another compound of similar polarity) is introduced through the same inlet system. This is of particular importance, because the beam time arrangement at a synchrotron facility is not very flexible, and the experiments need to be scheduled several months in advance. Therefore, only the unlabeled valeramide (**1**) and the deuterated compounds **1e** and **1g** were examined by PI.

Unlabeled acetamide (Merck) and valeramide **1** (Acros) were used as purchased. Labeled valeramides (Plate 1) were prepared in ca. 10 mmol scales as described in the following. The [*N*,*N*-D_2]-labeled compound **1a** was made by repetitive dissolution and subsequent evaporation of 0.5 g valeramide with 5 ml aliquots of CH_3OD (Janssen, 98 at.% D) until 94 at.% D incorporation was reached (two cycles). The other labeled amides were obtained by ammonolysis of the corresponding acid chlorides or esters with either aqueous or liquid ammonia in good to excellent yields (75–98%); tetrahydrofurane may be used as a convenient cosolvent. Because the PI experiments require samples of particularly high purities, all raw products were recrystallized from chloroform/hexane. Note that on a mmol scale this procedure is associated with considerable losses of sample as remainder in the mother liquor. Two well-established strategies were applied in the synthesis of the corresponding labeled valeric acids (and/or their derivatives) [17]. (i) C(2)–C(3) bond coupling is achieved by nucleophilic reaction of appropriately deuterated propyl bromides with the dianion of acetic acid ($-30\,^{\circ}C \rightarrow$ RT), where the latter is generated from acetic acid by addition of 2.1 eq. lithium diisopropylamide in tetrahydrofuran in the presence of 2.2 eq. dimethyl imidazolidone ($-30\,^{\circ}C \rightarrow 0\,^{\circ}C$). Subsequent work-up with 2N HCl, extraction, drying ($MgSO_4$), and bulb-to-bulb distillation leads to the corresponding acids in ca. 60% yield; this route was employed for the [2,2-D_2]- and [3,3-D_2]-compounds **1b** and **1c**. (ii) C(3)–C(4) bond coupling is achieved via Michael addition of appropriate ethyl Grignard reagents to ethyl acrylate (admixed with a four-fold excess of trimethylchloro silane) in the presence 5 mol% CuBr·Me_2S in order to prevent 1,2-addition [18]. Work-up with NH_3/NH_4Cl buffer (pH = 8), extraction, drying (Na_2SO_4), and bulb-to-bulb distillation leads to the corresponding ethyl esters in 60–80% yield, where the latter primarily depends on the purity of the labeled ethyl bromides used as precursors in the preparation of the Grignard reagents (see below). This route was applied for the [4-D_1]-, [4,4-D_2]-, [5,5,5-D_3]-, and [4,4,5,5,5-D_5]-compounds **1d–1g**. While **1d** was obtained as a racemic compound, the prefix *rac* is omitted for the sake of clarity. The labeled alkylbromides required in both routes were prepared by reduction of the corresponding acids (1.45 eq.), acid

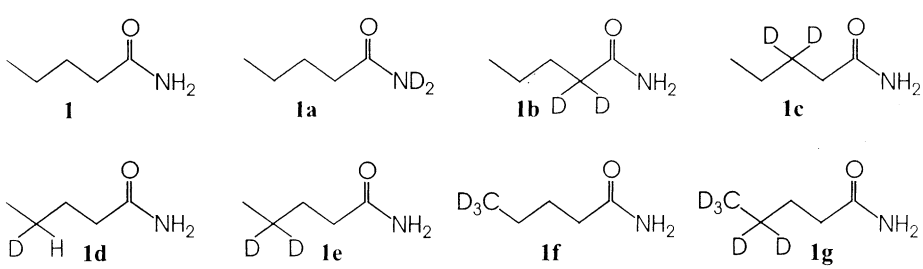

Plate 1.

chlorides (1.95 eq.), or aldehydes (3.6 eq.) with 1 eq. of either $LiAlH_4$ or $LiAlD_4$ (98 at.% D, Aldrich) in diethylether, followed by a direct work-up with 10 eq. concentrated HBr at −78 °C and gentle heating to 120 °C within an hour, while collecting the volatiles by distillation. Subsequent washing with water, then $NaHCO_3$, then brine, drying over $CaCl_2$ and redistillation affords the desired alkyl bromides in overall yields of 60–90% (based on deuterium). In this one-pot procedure, the otherwise troublesome isolation of the intermediate alcohols on a mmol scale is avoided. The products obtained via this route contain 2–10% of the corresponding symmetric dialkyl ethers, which do not disturb in the subsequent S_N2 or Grignard reactions, however.[1] Acryl-, vinylacet-, crotyl-, 2- and 3-bromopropionamides were made by ammonolysis of the corresponding esters. All products were spectroscopically characterized by GC-MS as well as ^{1}H-NMR, and isotopic purities were determined by CI-MS.

3. Results and discussion

The base peak in the 70 eV EI mass spectrum of valeramide [19] corresponds to $m/z = 59$ ($\Delta m = -42$; 100%) corresponding to the loss of propene via the McLafferty rearrangement. Other relevant fragments are due to losses of $CH_3^\bullet$ ($\Delta m = -15$; 5%), C_2H_4 ($\Delta m = -28$; 4%), and $C_2H_5^\bullet$ ($\Delta m = -29$; 24%), while the molecular ion at $m/z = 101$ is weak (1%) at 70 eV ionization energy. Notable increases in the relative abundances of the molecular ions have been observed upon ionization of amides with electrons having only 12 eV kinetic energy [20]. In order to analyze the underlying reaction mechanisms, the dissociation of ionized valeramide was examined by two different mass spectrometric techniques, i.e., MI studies using a sector-field mass spectrometer and PI experiments with synchrotron radiation both in conjunction with isotopic labeling techniques.

[1] Further purification of the alkyl bromides can easily be achieved by fractionation, but on small scales this procedure is associated with considerable losses of the volatile products.

3.1. Sector-field mass spectrometry

The mass-selected, MI $\mathbf{1}^{+\bullet}$ undergoes three major unimolecular transitions leading to the expulsions of ethene, ethyl radical, and propene, respectively, where the latter reaction corresponds to the McLafferty rearrangement. Three additional minor channels give rise to the elimination of methyl radical, ammonia, and water, respectively. For the sake of clarity, we classify these reactions as the C_1-, C_2- and C_3-channels, where C_1 comprises $CH_3^\bullet$ as well as the minute NH_3 and H_2O losses, C_2 summarizes ethene and ethyl expulsions, and C_3 stands for the loss of propene via the McLafferty rearrangement. Interestingly, the branching ratios between these channels not only depend on isotopic labeling, as expected, but also on the type of experiments being performed (see below). At first, let us analyze the labeling data in some detail in order to gain mechanistic insight. While not obvious at this point, it is important to note that the ionization conditions were adjusted to avoid CI and the source temperature was kept at 200 °C throughout the experiments described in this section.

C_3-route: The McLafferty rearrangement of $\mathbf{1}^{+\bullet}$ commences with γ-C–H bond activation to afford $\mathbf{2}^{+\bullet}$, a γ-distonic ion [21,22] which subsequently can undergo C–C bond cleavage to the ion/molecule complex $\mathbf{3}^{+\bullet}$ followed by loss of propene concomitant with the generation of the enol cation of acetamide $\mathbf{4}^{+\bullet}$ as ionic product (Scheme 1). As expected, the reaction proceeds with a high degree of selectivity in that more than 80% of the McLafferty products correspond to H(D) atom transfer from C(4). For example, a mass difference of $\Delta m = -43$ (loss of C_3H_5D) prevails for the [4,4-D_2]-compound **1e** (Table 1). Nevertheless, notable amounts of H/D exchange are observed which involve partial equilibrations of the H/D atoms at C(3), C(5), and the newly formed OH(D) group, whereas participations of the C(2) position, the remaining H/D atom at C(4), and the amino group are negligible. The participation of the aforementioned positions in H/D equilibration agrees nicely with previous results obtained for the interaction of propene with the ionized enol of acetic acid [23]. Scheme 1

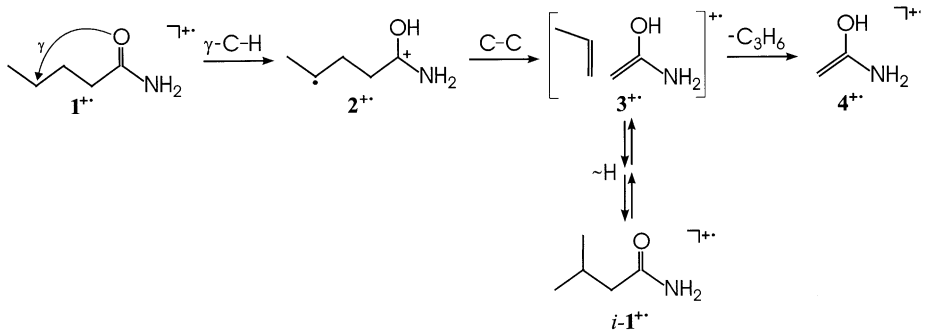

Scheme 1.

also suggests a possible scenario for the H/D exchange observed in the experiments by involving the transient formation of the isomeric amide cation ***i*-1**$^{+\bullet}$ within the lifetime of the ion/molecule complex **3**$^{+\bullet}$. Interestingly, the two formally identical methyl groups in ***i*-1**$^{+\bullet}$ do not participate equally in isotopic scrambling, i.e., **1c** shows slightly enhanced H/D equilibration compared to **1f**, although the latter compound has a higher deuterium content. This implies an asymmetry of the methyl groups in ***i*-1**$^{+\bullet}$ formed as a transient [24]. In fact, if the γ-hydrogen transfer ***i*-1**$^{+\bullet} \rightarrow$ **3**$^{+\bullet}$ is fast, it may effectively compete with the C–C bond rotation required for the involvement of the original C(5) position. This scenario is illustrated for **1c**$^{+\bullet}$ in Scheme 2.

As far as kinetic isotope effects (KIEs) are concerned, the observed H/D exchange processes do not permit a straightforward analysis of the ca. 2:3 ratio of C_3H_6 and C_3H_5D losses from the [4-D_1]-compound **1d**, because H/D equilibration via ***i*-1d**$^{+\bullet}$ only contributes to the C_3H_5D loss. Prior to the detailed kinetic modeling presented below, one can therefore only conclude that the KIE associated with the hydrogen migration in the McLafferty rearrangement is $\leq$1.5. Another notable aspect is the decrease of the C_3-route for the [3,3-D_2]-compound **1c**, which

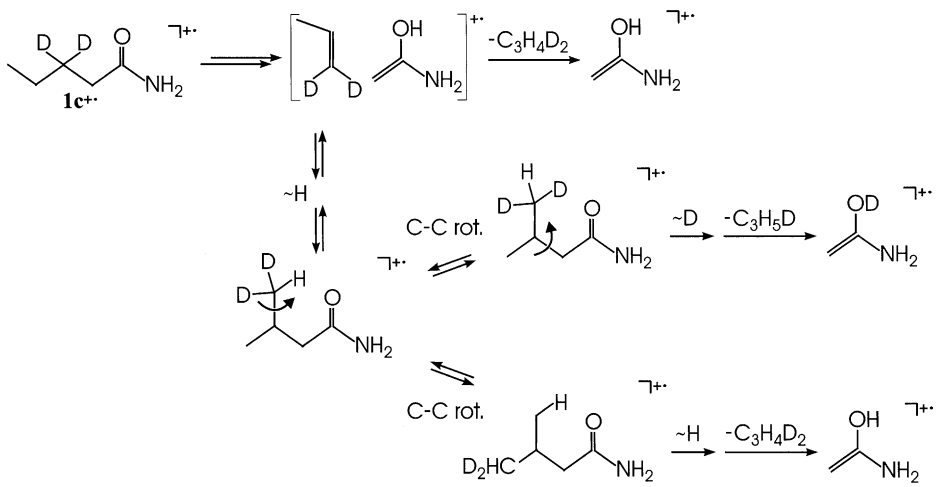

Scheme 2.

implies the operation of a secondary KIE associated with C(2)–C(3) bond cleavage in the McLafferty rearrangement. [2]

C_2-route: In contrast to the McLafferty rearrangement, the C_2-channel shows extensive H/D equilibrations. The product distributions are, however, far from being statistical and seem to follow some distinct mechanistic scenario. For a more straightforward analysis, the ethene and ethyl losses need to be deconvoluted at first. Inspection of the experimental data reveals that loss of ethene proceeds specifically from the C(4) and C(5) positions as suggested by the negligible intensity of $\Delta m = -28$ for the terminally deuterated compounds **1d**–**1g**; for the same reason, unimolecular loss of carbon monoxide (also $\Delta m = -28$) can be ruled out. Accordingly, the remaining product pattern associated with the loss of ethyl radical can be analyzed. A key assumption for the mechanistic understanding is that in addition to the McLafferty rearrangement, the ionized carbonyl compound can competitively undergo δ-C–H bond activation leading initially to the δ-distonic ion $\mathbf{5}^{+\bullet}$ which serves as a key intermediate in the C_2-route (Scheme 3). Subsequent C(3)–C(4) bond cleavage of $\mathbf{5}^{+\bullet}$ explains the selective loss of ethene from the terminal positions with the β-distonic ion $\mathbf{6}^{+\bullet}$ as a plausible ionic product (see below); for the corresponding β-distonic derivative with a methoxy instead of an amino substituent [26]. Interaction of the radical and the charged center in $\mathbf{5}^{+\bullet}$ via the cyclic structure c-$\mathbf{5}^{+\bullet}$ (either as a minimum or as a saddle point) can promote a degenerate rearrangement which results in the pair-wise equilibration of the methylene groups at C(2)/C(3) with C(4)/C(5). Note, however, that the loss of ethene only occurs as a direct process. Hence, those ions whose internal energy content is low enough to permit degenerate rearrangement within the ions lifetime do not undergo loss of ethene. In addition, the distonic ion $\mathbf{5}^{+\bullet}$ can undergo a 1,4-hydrogen transfer to yield the α-distonic ion $\mathbf{7}^{+\bullet}$ which is equivalent to the ionized enol of valeramide. Intermediate $\mathbf{7}^{+\bullet}$ may then be regarded as an ideal precursor for ethyl loss, because the formation of protonated acrylamide $\mathbf{8}^{+}$ is considered to provide an energetically favorable exit channel [27]. While the resulting mechanistic scenario involving $\mathbf{5}^{+\bullet}$ as a key intermediate explains almost all labeling data of the C_2-route, an additional channel needs to be involved. For the terminally deuterated compounds **1f** and **1g** significant amounts $\Delta m = -32$ and -34, respectively, are observed which indicate some losses of the intact ethyl groups. Based upon energetic considerations [27], we suggest that C–C bond cleavage is associated with C–O bond formation leading to the cyclic immonium ion $\mathbf{9}^{+}$. While simple C–C bond cleavage of $\mathbf{1}^{+\bullet}$ cannot be excluded, it appears unfavorable because the primary carbocation $\mathbf{10}^{+}$ needs to be formed which is considered unstable [27].

A key aspect in Scheme 3 is the equilibration of the methylene groups at C(2)/C(3) with C(4)/C(5) via structure c-$\mathbf{5}^{+\bullet}$. Because this situation is quite complex, let us discuss in some detail the results for the [2,2-D_2]-compound **1b** as an illustrative example (Scheme 4). Direct C–C bond cleavage ($\mathbf{1b}^{+\bullet} \rightarrow \mathbf{9b}^{+}$) gives rise to loss of an intact ethyl radical from the terminus, $\Delta m = -29$. The competing δ-C–H bond activation affords the distonic ion $\mathbf{5b}^{+\bullet}$, from which another direct C–C bond cleavage ($\mathbf{5b}^{+\bullet} \rightarrow \mathbf{6b}^{+}$) leads to the expulsion of unlabeled ethene, $\Delta m = -28$. The two major C_2-channels of $\mathbf{1b}^{+\bullet}$ are due to the indirect C_2-route via 1,4-D(H) transfer ($\mathbf{5b}^{+\bullet} \rightarrow \mathbf{7b}^{+\bullet}$ and $\mathbf{5b'}^{+\bullet} \rightarrow \mathbf{7b'}^{+\bullet}$). However, formation of the enol cation $\mathbf{7b}^{+\bullet}$ (which subsequently leads to loss of a $C_2H_4D^{\bullet}$ radical, $\Delta m = -30$) requires a 1,4-D transfer. Instead, the degenerate rearrangement via c-$\mathbf{5b}^{+\bullet}$ leads to the isotopolog $\mathbf{5b'}^{+\bullet}$ from which 1,4-H transfer can occur to subsequently afford $\mathbf{7b'}^{+\bullet}$, followed by the elimination of $C_2H_3D_2^{\bullet}$ ($\Delta m = -31$). The experimentally observed preference for $\Delta m = -31$ therefore indicates the operation of a KIE, not in the initial δ-C–H bond activation $\mathbf{1}^{+\bullet} \rightarrow \mathbf{5}^{+\bullet}$, but nevertheless in the reaction $\mathbf{5}^{+\bullet} \rightarrow \mathbf{7}^{+\bullet}$ occurring prior to dissociation; similar situations have been coined "hidden" hydrogen rearrangements [28,29]. In fact, the experimental results point towards a complete equilibration of $\mathbf{5b}^{+\bullet}$ and

[2] For a detailed analysis of KIEs operative in the McLafferty rearrangement of ketones [25].

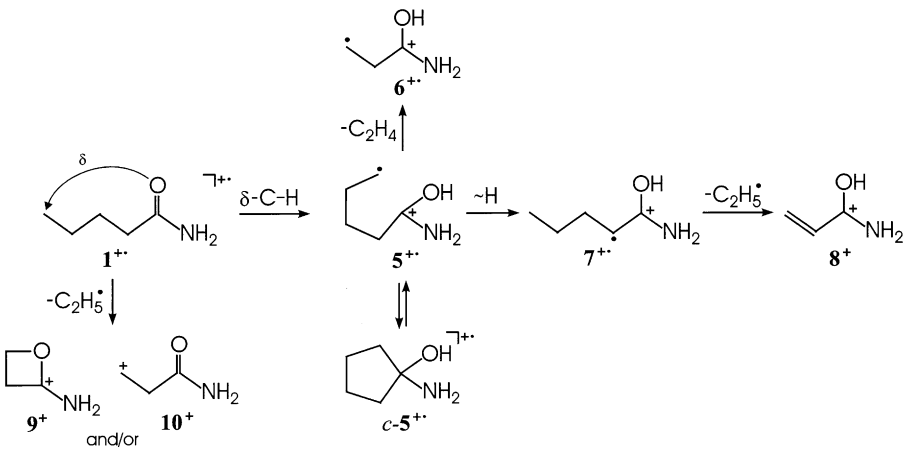

Scheme 3.

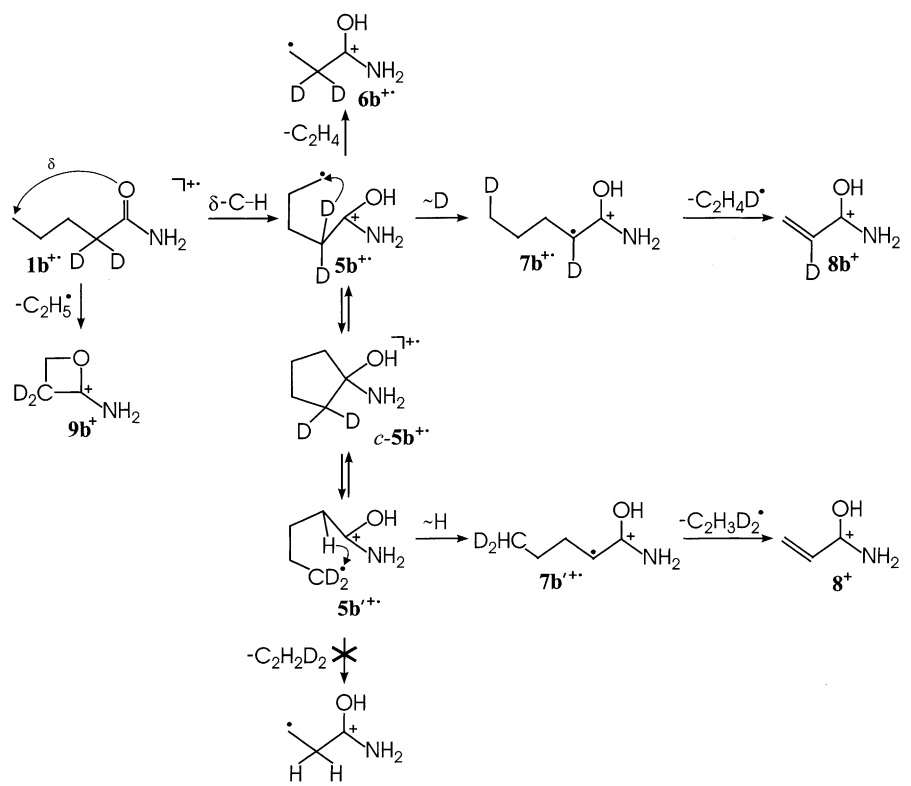

Scheme 4.

$\mathbf{5b}'^{+\bullet}$ in the present case (see below). Further, a significant KIE associated with δ-C–H bond activation is implied by the reduced amounts of the C_2-channels for the terminally labeled compounds **1f** and **1g**. As both C_2- and C_3-routes are affected by deuteration in **1g**, the observed decrease of the C_2-channel relative to C_3 further indicates KIE(δ-CH) > KIE(γ-CH).

Due to the complexity of the mechanistic scheme, the KIEs cannot directly be derived from the experimentally observed intensity patterns and require a more comprehensive, detailed analysis instead. If H/D equilibration as well as KIEs are taken into account, however, the reactions depicted in Scheme 3 can rationalize the complete labeling distributions observed for the C_2-route reasonably well (see below). An essential aspect of the whole scenario is the fact that the pronounced H/D equilibration in the C_2-route (though far from being statistical) is *not* reflected in the McLafferty products. While some H/D exchange is obvious in the C_3-route, the C(2) position, for example, does not participate in that loss of unlabeled propene ($\Delta m = -42$) occurs almost exclusively for $\mathbf{1b}^{+\bullet}$. In fact, the labeling data indicate that the intermediates formed via γ- and δ-C–H bond activations are effectively uncoupled from each other and do not interconvert. This conclusion is of prime importance for the understanding of the variations in the C_3/C_2 ratios, and it will be discussed further below in quite some detail.

C_1-route: The three minor channels observed correspond to losses of $CH_3^\bullet$, NH_3, and H_2O, respectively. The latter is minuscule and is, therefore, not pursued anymore. The labeling distributions indicate that neutral ammonia is primarily formed from the intact amino group and a hydrogen atom from C(3). However, this channel is not analyzed in further detail, due to the low abundance and interferences with ^{13}C-isotopes of the $[M - H]^+$ ions (see experimental section). As far as methyl loss is concerned, the data indicate high preference for loss of the terminal position. Specifically, $\Delta m = -15$ almost vanishes for **1f** and **1g** and is shifted to $\Delta m = -18$, corresponding to losses of $CD_3^\bullet$; some remainder at $\Delta m = -15$ indicates that more complex rearrangements occur to a small extent. Interestingly, loss of methyl decreases to about a half upon deuteration of the C(3) position, thus indicating the operation of a significant KIE in this particular process. By analogy to the competition of γ-C–H and δ-C–H bond activation in the major channels, we therefore propose that methyl loss emerges from β-C–H bond activation (Scheme 5). The so-formed β-distonic ion $\mathbf{11}^{+\bullet}$ can subsequently undergo C–C bond cleavage to liberate a methyl radical concomitant with the formation of protonated vinylacetamide $\mathbf{12}^+$ [20].

Kinetic modeling: According to the above analysis, five major channels compete in the unimolecular dissociation of ionized valeramide. (i) Cleavage of the β-C–C bond in $\mathbf{1}^{+\bullet}$ leads to the direct loss of $C_2H_5^\bullet$ concomitant with the formation of the cyclic species $\mathbf{9}^+$ and/or, though far less likely, $\mathbf{10}^+$, (ii) β-C–H bond activation that results in the elimination of $CH_3^\bullet$, (iii) γ-C–H bond activation initiates the McLafferty rearrangement, and δ-C–H bond activation gives rise to the distonic ion $\mathbf{5}^{+\bullet}$ from which (iv) C_2H_4 and (v) the "indirect" $C_2H_5^\bullet$ losses evolve. Quite obviously, these reactions compete with each other, and any labeling will affect the branching ratios due to the operation of KIEs. In such a situation, even small intrinsic KIEs may give rise to huge variations in the measured product distributions. Depending on the size of the KIEs, this may lead to extremely large (or small) apparent KIEs [30]. While competition due to the C_1-route may certainly be neglected in the present case, any appropriate quantitative analysis must account for the competition of the four other channels.

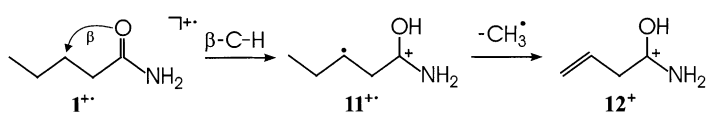

Scheme 5.

Accordingly, a kinetic modeling was performed in which each fragmentation reaction is described by a relative rate constant, the associated KIEs, and additional parameters accounting for the H/D exchange processes observed (Appendix A). The resulting sets of equations have many unknown variables, and in order to achieve a physically meaningful solution, reasonable starting parameters and boundary conditions are first to be derived from experiment. To this end, let us analyze the experimental data more thoroughly. Neglecting the minor channels (<1%), **1** and **1a** thus provide the relative rate constants $k(CH_3^\bullet) = 2$, $k(C_2H_4) = 7$, $k(C_2H_5^\bullet)_{direct} + k(C_2H_5^\bullet)_{indirect} = 42$, and $k(C_3H_6) = 49$ as reference points. According to the mechanistic schemes suggested above, $k(CH_3^\bullet)$, $k(C_2H_4)$, and $k(C_2H_5^\bullet)_{direct}$ are assumed to remain constant for **1b**, whereas $k(C_2H_5^\bullet)_{indirect}$ and $k(C_3H_6)$ may be changed due to a primary KIE operative in the H(D) transfer $\mathbf{5}^{+\bullet} \rightarrow \mathbf{7}^{+\bullet}$ and a secondary KIE associated with C(2)–C(3) bond cleavage in the McLafferty rearrangement ($\mathbf{2}^{+\bullet} \rightarrow \mathbf{3}^{+\bullet}$), respectively. The following conclusions can be derived from consideration of the experimental data for **1b**. The similar abundances of the signals at $\Delta m = -28$ and -29, corresponding to the direct losses of C_2H_4 and $C_2H_5^\bullet$, respectively, suggest $k(C_2H_4) \approx k(C_2H_5^\bullet)_{direct}$. Further, the decrease of $k(C_2H_5^\bullet)_{indirect}$ (represented by the sum of the signals at $\Delta m = -30$ and -31) indicates that upon deuteration of the C(2) position the primary KIE ($\mathbf{5}^{+\bullet} \rightarrow \mathbf{7}^{+\bullet}$) prevails over the secondary KIE associated with the C_3-channel. Likewise, inspection of the data for **1c** points to the operation of (i) a primary KIE on $k(CH_3^\bullet)$, denoted as KIE(β-CH), (ii) a secondary KIE on $k(C_2H_4)$ and (iii) a secondary KIE on $k(C_3H_6)$. As the overall C_3/C_2 ratio for **1c** decreases relative to the unlabeled system, it is further implied that the secondary KIE on $k(C_3H_6)$ exceeds those associated with $k(C_2H_5^\bullet)$ for this particular compound. Further, the signal for $\Delta m = -43$ indicates occurrence of some H/D exchange in the McLafferty route, whereas the participation of C(3) in the H/D exchange of the C_2-route, giving rise to the weak signal at $\Delta m = -30$, is neglected. For the next two compounds **1d** and **1e**, minor changes in the overall C_3/C_2 ratios may indicate a small primary KIE operative in the McLafferty route, KIE(γ-CH). To a very first approximation, the ratio of $\Delta m = -42$ and -43 obtained for **1d** implies KIE(γ-CH) = 1.5, but H/D exchange needs to be incorporated because it only contributes to the $\Delta m = -43$ (see above). For **1f**, the decrease of the overall C_2-channel indicates a primary KIE in this route, KIE(δ-CH). Finally, the data of **1g** suggest KIE(δ-CH) > KIE(γ-CH) as well as some H/D exchange between C(2) and C(5) in the C_2-route (see above). Again, both **1f** and **1g** also show some H/D exchange in the McLafferty products. Instead of a rigorous analysis, H/D scrambling in the different routes is described phenomenologically by the associated KIE(H/D, C_2) and KIE(H/D, C_3) as well as parameters x_{scr}, where the latter stand for the participation of the relevant positions in H/D equilibration, i.e., C(2) and C(5) for the C_2-route and C(3), C(5), and OH(D) for the C_3-route.

While the parameters derived from the unlabeled system were kept constant and the boundary conditions were acknowledged, all other variables were then fitted to the product distributions given in Table 1 using least square criteria. Using these restrictions, the set of equations appears to have a single solution which leads to the intensities given in Table 2 with the parameters indicated (see Appendix A for further details). Although by no means perfect, the kinetic modeling reproduces the experimental data reasonably well, and the maximal deviations are clearly within experimental uncertainty. Of course, much better fits can be obtained, when additional variables are introduced, but this would increase the risk of multiple solutions for the set of equations. Moreover, the modeling might become self-fulfilling by basically introducing a separate parameter for each process. In fact, we deliberately followed the opposite approach by minimizing the number of parameters as much as possible to those which are mechanistically most insightful and those required for a reasonable fit of the data.

The most important result of the fitting is that the proposed mechanistic schemes can reproduce the experimentally observed fragmentation patterns quite well. Hence, two mechanistic conclusions evolve.

Table 2
Modeled intensities[a,b,c] and branching ratios of C_1-, C_2-, and C_3-channels[d] for $\mathbf{1}^{+\bullet}$ and its isotopologs where the deviations from the data presented in Table 1 are given behind the dashes[e]

	C_1[d]	−15	−18	C_2[d]	−28	−29	−30	−31	−32	−33	−34	C_3[d]	−42	−43	−44	−45	−46	−47
1	2/±0	2/±0	<1[b]	49/±0	7/±0	42/±0						49/±0	49/±0	–[g]/±0				
1a	2/±0	2/±0	<1[b]	49/±0	7/±0	42/±0	–[f]/±0					49/±0	49/±0	–[h]/±0	–[h]/±0			
1b	3/+1	2/±0	<1[b]	45/±0	8/+1	8/+1	12/±0	17/−2				53/±0	53/±0					
1c	2/+1	1/±0	<1[b]	52/±0	7/+2	27/−2	–[f]/−1	18/+1				47/±0	–[h]/±0	7/±0	40/±0			
1d	2/±0	2/±0	<1[b]	51/+1	–[f]/±0	25/±0	26/+1					47/−1	18/−1	29/±0				
1e	2/±0	2/±0	<1[b]	52/−1		18/−3	8/+1	26/+1				46/±0		38/±0	8/±0			
1f	3/±0	<1[b]	2/±0	40/−1	–[f]/±0		16/+1	15/±0	9/−2			57/+1		–[h]/±0	7/−1	50/+2		
1g	3/±0	<1[b]	2/±0	43/+1		–[f]/±0	8/+1	2/±0	9/±0	14/±0	10/±0	54/−1		–[h]/±0			50/−1	4/±0

[a] Normalized to $\Sigma = 100$.

[b] No deviations are given for channels <1, and for the same reason, the columns for $\Delta m = -17$ and -19 are omitted (Appendix A).

[c] The following relative rate constants, KIEs, and other parameters are used in the modeling. Rate constants: $k(CH_3^{\bullet}) = 2.0$, $k(NH_3) = 0.2$, $k(H_2O) = 0.1$, $k(C_2H_4) = 7.0$, $k(C_2H_5^{\bullet})_{direct} = 7.7$, $k(C_2H_5^{\bullet})_{indirect} = 34.0$, and $k(C_3H_6) = 49.0$. Primary H/D KIEs: KIE(β-CH) = 1.7, KIE(γ-CH) = 1.01, KIE(δ-CH) = 1.3, KIE(H/D, C_2) = 1.8, and KIE(H/D, C_3) = 1.9, where KIE(H/D, C_2) is operative in the 1,4-H(D) transfer $\mathbf{5}^{+\bullet} \rightarrow \mathbf{7}^{+\bullet}$ of the C_2-route, and KIE(H/D, C_3) affects the H/D equilibration in the C_3-route. Of the secondary KIEs conceivable, only the one resulting from perdeuteration at C(3) in the C–C bond cleavage KIE(C(3), C_3) = 1.12 needs to be acknowledged. Other parameters: 10:1 ratio of specific vs. non-specific $CH_3^{\bullet}$ losses, $x_{scr} = 0.16$ for the H/D exchange between C(2) and C(5) in the indirect loss of $C_2H_5^{\bullet}$, $x_{scr} = 0.28$ for the H/D exchange between C(3), C(5), and OH(D) in the McLafferty rearrangement with a 54:46 preference for participation of C(3) vs. C(5).

[d] See footnote b of Table 1.

[e] The average deviation is ±4; the largest deviations occur in the C_2-channel; the maximum is −3.3 for $\Delta m = -29$ from **1e**.

[f] Losses of these isotopically scrambled C_2-fragments are not included in the modeling.

[g] $\Delta m = -43$ from $\mathbf{1}^{+\bullet}$ is not included in the modeling.

[h] Eliminations of these isotopically scrambled C_3-fragments are not included in the modeling.

At first, a satisfactory modeling lends support to the suggestion that the C_2- and C_3-routes compete in the dissociation of $\mathbf{1}^{+\bullet}$. However, the associated γ- and δ-C–H bond activations occur more or less irreversibly, namely, the intermediate distonic ions of the C_2- and C_3-routes are uncoupled from each other. Secondly, the behavior of ionized valeramide can be described without invoking skeletal rearrangements initiated by 1,2-migrations of the $CONH_2$ entity, which is in marked contrast to the facile 1,*n*-migrations of carboxy groups in the cation radicals of the related carboxylic acids [5,6,31]. Finally, the kinetic modeling leads to the following values of the primary KIEs associated with the various H(D) migrations (values and errors derived from the refined model, see Appendix A). For the initial C–H bond activations, rather small isotope effects evolve: KIE(β-CH) ≈ 1.6, KIE(γ-CH) = 1.03 ± 0.07, and KIE(δ-CH) = 1.32 ± 0.11; in fact, KIE(γ-CH) = 1.03 ± 0.07 disputes a rate-determining 1,5-H migration in the McLafferty rearrangement. Significantly larger KIEs are obtained for the subsequent steps, i.e., KIE(H/D, C_2) = 2.0 ± 0.6 associated with the 1,4-H(D) migration $\mathbf{5}^{+\bullet} \rightarrow \mathbf{7}^{+\bullet}$ and KIE(H/D, C_3) ≈ 1.9 operative in the partial H/D equilibration of intermediate $\mathbf{3}^{+\bullet}$.

Fragment ions: In order to probe the mechanistic conclusions derived above, the dissociation patterns of the resulting fragment ions are addressed comprehensively in this section. However, instead of probing the fragments formed upon unimolecular dissociation of mass-selected $\mathbf{1}^{+\bullet}$ in subsequent collisions, we have chosen to concentrate on the unimolecular dissociations of the fragment ions formed by dissociative EI of valeramide in the ion source for two reasons. (i) Even upon collisional activation, the dissociation patterns of the fragments considered here are dominated by unimolecular processes. [3] (ii) Due to too low abundancies, characterization of the minor fragment ions (e.g., $CH_3^\bullet$ loss) generated from metastable $\mathbf{1}^{+\bullet}$ is impossible. Further, these experiments were conducted in a CI source in order to allow direct comparison with reference ions generated independently (see below).

C_3-route: Mourgues et al. [32] already have demonstrated by using ion/molecule reactions that the McLafferty rearrangement upon dissociative EI of carboxamides gives rise to the enol cation $\mathbf{4}^{+\bullet}$. Fragmentation of $\mathbf{4}^{+\bullet}$, however, occurs via intramolecular rearrangement to the keto form, i.e., ionized acetamide, prior to dissociation followed by competing α-cleavages to yield $CH_3CO^+ + NH_2^\bullet$ and $CH_3^\bullet + CONH_2^+$, respectively. The experimental data are in full accord with this scenario (Table 3). For unlabeled $\mathbf{4}^{+\bullet}$, losses of $CH_3^\bullet$ ($\Delta m = -15$) and $NH_2^\bullet$ ($\Delta m = -16$) are observed in a ca. 2:1 ratio. For the latter, a clean shift to $ND_2^\bullet$ ($\Delta m = -18$) is observed for the [*N*,*N*-D_2]-labeled ion $\mathbf{4a}^{+\bullet}$ in conjunction with a slight decrease of this channel due to a secondary KIE. Likewise, the [2,2-D_2]-labeled ion $\mathbf{4b}^{+\bullet}$ shows losses of $NH_2^\bullet$ ($\Delta m = -16$) and $CHD_2^\bullet$ ($\Delta m = -17$). Losses of $CH_2D^\bullet$ and $NH_2^\bullet$ coincide at $\Delta m = -16$ for the [*O*-D]-labeled ion $\mathbf{4e}^{+\bullet}$ generated from either **1e** or **1g**. We note in passing that for all isotopologs studied losses of CO and $HCCO^\bullet$ occur as side reactions which are particularly pronounced for ionized acetamide itself (Table 3) [11,33].

C_2-route: The analysis of this route is most difficult, because loss of ethene as well as direct and indirect losses of ethyl radical compete with each other, and isobaric interferences due to the natural abundance of ^{13}C are to be considered. Further, the branching of these routes is quite different upon dissociative EI compared to the dissociations of metastable $\mathbf{1}^{+\bullet}$ in that the direct $C_2H_5^\bullet$ loss from the terminus is much more pronounced in the former. For example, the mass region corresponding to losses of $\Delta m = -28$ to -32 in the 70 eV EI mass spectrum of **1f** shows a pattern of 8:1:10:34:100, hence, loss of $C_2D_5^\bullet$ ($\Delta m = -32$) gives rise to the most prominent peak in the C_2-region, whereas loss of $C_2D_5^\bullet$ constitutes a minor route for metastable $\mathbf{1f}^{+\bullet}$.

The MI spectrum of the $m/z = 73$ ion from the unlabeled compound (corresponding to loss of C_2H_4,

[3] This is also a consequence of the experimental set-up [12], which has an unusually long (1.9 m) field-free region between *E*(1) and *B*(2), where the experiments were performed such that unimolecular dissociations also predominate in the collisional activation spectra.

Table 3
Mass differences (Δm in amu) observed in the MI spectra of $B(1)/E(1)$ mass-selected fragment ions generated by dissociative EI of valeramide and its isotopologs and the MI spectra of independently generated reference ions[a,b]

Precursor	m/z[c]	−1	−2	−15	−16	−17	−18	−19	−20	−28	−29	−30	−31	−43	−44
C_3-route															
1	59			100	43	5				10					
1a	61			100			33	2		11					
1b	61				50	100	1	2		13					
1e/1f	60				100	1	2			3					
Acetamide[d,e]	59			100	32	8	1			97					
C_2-route															
1	72					100				4					
	73	100			10	28	1				2				
1a	74						2	100		4					
	75	100					8	30	3						
1b	72					100				4					
	74					100	5			5					
	75	100	16		18	33	8						4		
1c	74					57	100	1		7					
	75	100	14		14	20	13	1				1	3		
1f	72					100				5					
	74	100	6		14	25	10	1				4			
Acrylamide[f]	72					100				2					
2-Br-propionamide[f]	72					100				10					
3-Br-propionamide[f]	72					100				2					
C_1-route															
1	86					19				8	2			100	
1a	88						1	18		2	1			14	100
1b	88					11	1			7	0			100	5
1c	88					4	5			9	2			100	2
1e/1g	88					10	3			6	1			100	5
Vinylacetamide[f]	86					3				1				100	
Crotylamide[f,g]	86					100				1				1	
Methacrylamide[f]	86					100				23				1	

[a] Relative to the base peak (100%); signals <1% are omitted.
[b] The other labeled valeramides gave similar results and are omitted for the sake of brevity.
[c] Mass of the fragment ion selected.
[d] Formation of NH_4^+ concomitant with loss of HCCO$^\bullet$ (and the corresponding isotopologs) is also observed to some extent (5–10%).
[e] EI, 70 eV.
[f] Chemical ionization with CH_4 as reagent gas.
[g] 97% *E*-derivative.

$\Delta m = -29$) is dominated by expulsion of a hydrogen atom ($\Delta m = -1$) concomitant with some losses of $NH_2^\bullet$ and NH_3 ($\Delta m = -16$ and -17, respectively), where the assignment of the two latter neutrals follows from the data for **1a**. Elimination of open-shell neutrals is characteristic for cation radicals, and thereby consistent with the suggested fragment ion structure $\mathbf{6}^{+\bullet}$. As far as the origin of the hydrogen atom is concerned, except the amino group, all other positions contribute to hydrogen atom loss, i.e., expulsions of D$^\bullet$ ($\Delta m = -2$) occur for $m/z = 74$ from **1f** as well as for $m/z = 75$ from **1b** and **1c**, respectively. The lack of specificity in H-atom loss indicates structural flexibility of the fragment in that $\mathbf{6}^{+\bullet}$ seems to be able to easily undergo isomerizations. For this particular fragment ion, no suitable precursors were found to independently generate reference ions.

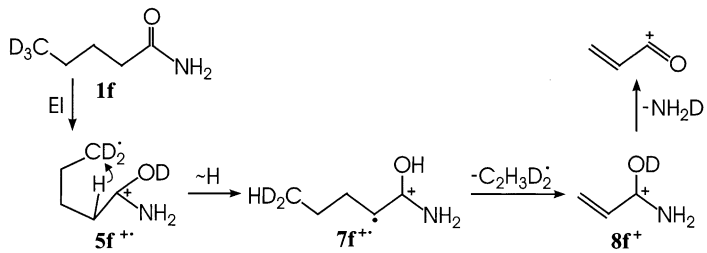

Scheme 6.

As far as the elimination of ethyl radical is concerned, the MI spectrum of the $m/z = 72$ ion resulting from the unlabeled compound **1** (corresponding to loss of $C_2H_5^{\bullet}$, $\Delta m = -29$) shows mass differences of $\Delta m = -17$ (100%) and -28 (4%), which change to $\Delta m = -19$ (100%) and -28 (4%) for the $m/z = 74$ ion generated from the [*N*,*N*-D_2] compound **1a**. Accordingly, these reactions correspond to losses of ammonia and C_2H_4, respectively; extrusion of CO can be excluded from the mass shifts of the other labeled fragment ions. Note that for **1** and **1a** as precursors, $\Delta m = -29$ corresponds to a mixture of direct and indirect $C_2H_5^{\bullet}$ eliminations. Differentiation of these routes is feasible for compounds **1b** and **1f**, which can only yield $m/z = 72$ via indirect and direct ethyl losses, $\Delta m = -29$ and -32, respectively. The corresponding MI spectra are very similar to each other with predominating elimination of NH_3 and a small amount of C_2H_4 loss (also the collisional activation spectra of these ions do not differ largely). Hence, either the direct and indirect routes lead to the same products or the isomeric fragments interconvert easily. Based upon a previous theoretical study [27], we tend to prefer the latter option.

Let us now attempt to analyze the mechanistic pictures suggested above by reference to the labeled fragment ions. Accordingly, loss of $C_2H_3D_2^{\bullet}$ from **1f** can only occur via the indirect route to yield the [*O*-D]-labeled ion $\mathbf{8f}^+$ (Scheme 6). The MI spectrum of the resulting fragment ion ($m/z = 73$ from **1f**) is consistent with this suggestion in that elimination of NH_2D ($\Delta m = -18$) predominates. On the other hand, loss of $C_2H_5^{\bullet}$ from **1b** must arise from the direct route. The corresponding MI spectrum ($m/z = 74$ from **1b**) is dominated by the elimination of NH_3, though some participation of the C(2) position is indicated by some elimination of NH_2D ($\Delta m = -18$). A connection between both routes is provided by the $m/z = 74$ ion generated from **1c** which constitutes a mixture resulting from the direct and indirect $C_2H_5^{\bullet}$ eliminations. For this ion, losses of NH_3 and NH_2D are observed in a ca. 1:2 ratio of which the former is attributed to the indirect route and the latter stems from the direct variant.

Comparison with independently generated reference ions lends support to this scenario. Thus, loss of NH_3 prevails for protonated acrylamide as well as for the [M + H^+–HBr] ions generated from 2- and 3-bromopropionamide, respectively. For the two latter, $\Delta m = -28$ is somewhat enhanced, probably due to higher internal energy contents of these precursor ions.

C_1-route: Unimolecular dissociation of the $m/z = 86$ ion generated from the unlabeled compound (corresponding to loss of $CH_3^{\bullet}$ from $\mathbf{1}^{+\bullet}$, $\Delta m = -15$) shows mass differences of $\Delta m = -17$ (19%), -28 (8%),[4] -29 (2%), and -43 (100%). In this fortunate case, it is entirely sufficient to concentrate on the base peak [10]. Thus, for the independently generated reference ions, $\Delta m = -43$ as the base peak is only observed for protonated vinylacetamide, whereas losses of ammonia prevail for protonated crotyl- and methacrylamide. Thus, comparison to the isomers

[4] The labeling data suggest that $\Delta m = -28$ corresponds primarily to loss of CO. This process gives rise to a bimodal peak shape because one of the reactions is associated with a considerable kinetic energy release (most pronounced in the MI spectrum of protonated methacrylamide).

nicely confirms the suggested formation of structure $\mathbf{12}^+$ as derived from the labeled valeramide ions. As far as the nature of the ionic and neutral fragment associated with $\Delta m = -43$ from the $m/z = 86$ ion is concerned, the labeling data (Table 3) suggest the formation of a $C_3H_7^+$ cation concomitant with loss of neutral HNCO, which is consistent with the slightly larger gas phase basicity of propene (172.6 kcal/mol) compared to HNCO (171.7 kJ/mol) [34].

3.2. Photoionization (PI) experiments

At photon energies sufficiently above threshold, the PI mass spectrum of valeramide very much resembles the EI spectrum. With 20 eV photons, for example, loss of propene ($\Delta m = -42$) gives rise to the base peak (100%), whereas eliminations of $CH_3^\bullet$ ($\Delta m = -15$, 3%), C_2H_4 ($\Delta m = -28$, 2%), and $C_2H_5^\bullet$ ($\Delta m = -29$, 17%) as well as the molecular ion (4%) bear much weaker signals. Above 12 eV photon energy, also typical α-cleavage products (e.g., $CONH_2^+$, $m/z = 44$) are observed which are not pursued any further. Fig. 1 summarizes the variations of the relevant fragment ions with photon energy. The first notable aspect is that even at the onset of PI some fragmentation due to the McLafferty rearrangement ($\Delta m = -42$) is observed, indicating a rather low activation barrier of this particular process.

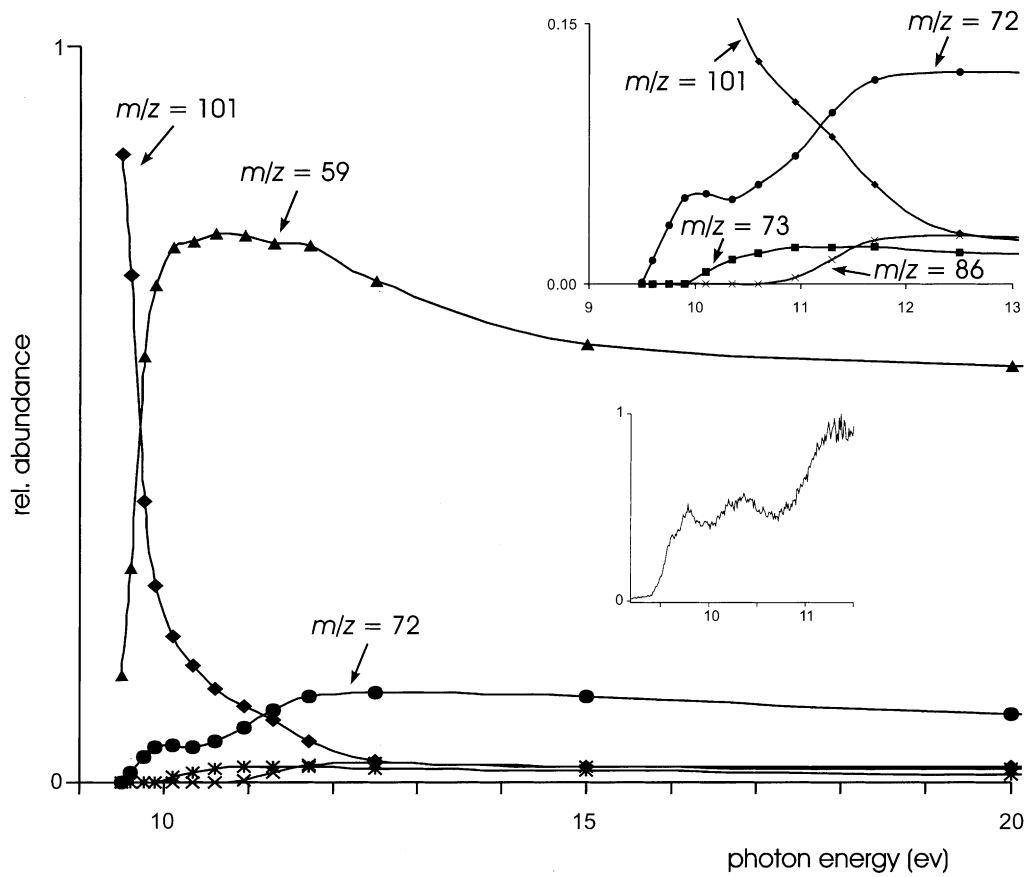

Fig. 1. Breakdown diagram for the photoionization of valeramide **1** at different photon energies. Only the parent (◆) and the fragments ions due to losses of $CH_3^\bullet$ (×), C_2H_4 (■), $C_2H_5^\bullet$ (●), and C_3H_6 (▲), respectively, are shown. The data are normalized to $\Sigma = 1$ for all ions observed, including the α-cleavage products formed above 12 eV photon energy.

Already at 9.6 eV photon energy, also elimination of ethyl ($\Delta m = -29$), corresponding to the appearance of the C_2-channel, is observed. The losses of C_2H_4 and $CH_3^\bullet$ are first visible in the PI spectra at 10.1 and 10.9 eV, respectively. Further, the energy-dependence of the C_2H_4 and $C_2H_5^\bullet$ channels supports the competition of the two direct reactions $\mathbf{1}^{+\bullet} \rightarrow \mathbf{6}^{+\bullet} + C_2H_4$ and $\mathbf{1}^{+\bullet} \rightarrow \mathbf{9}^{+} + C_2H_5^\bullet$ with the indirect route $\mathbf{1}^{+\bullet} \rightarrow \mathbf{8}^{+} + C_2H_5^\bullet$ as suggested above. Thus, at low photon energies, the C_2-route can only proceed via indirect $C_2H_5^\bullet$ loss giving rise to a continuous increase of the trace for $\Delta m = -29$ (see upper inset in Fig. 1). At about 10 eV, a change in slope is observed which can be attributed to competition with the loss of ethene, i.e., the onset of the trace for $\Delta m = -28$. At about 10.5 eV, the intensity of the $\Delta m = -29$ fragment starts to increase again. A plausible rational is the accessibility of the direct $C_2H_5^\bullet$ loss (see above), perhaps due to the fragmentation of electronically excited $\mathbf{1}^{+\bullet}$. Note that the apparent thresholds of these minor channels can only be regarded as upper limits, because the strongly competing C_3-route as well as the indirect $C_2H_5^\bullet$ loss are likely to cause substantial kinetic shifts of the more energy demanding channels. For the three major ions, separate scans using single-ion monitoring yield refined appearance energies of $AE(\mathbf{1}^{+\bullet}) = 9.40 \pm 0.03$ eV, $AE(\mathbf{4}^{+\bullet}) = 9.43 \pm 0.05$ eV, and $AE(\mathbf{8}^{+}) = 9.58 \pm 0.05$ eV. Hence, both the C_2- and the C_3-routes appear to be associated with rather low activation barriers such that the thermal energy of the neutral valeramide in conjunction with the energy imparted upon PI is sufficient to cause ion dissociation in the μs regime. In marked contrast to the MI data obtained with the sector instrument, however, the overall C_3/C_2 branching ratio is changed from about 1 in the sector experiments to >5 upon PI, even at the largest photon energies examined.

As far as PI of **1** is concerned, $AE(\mathbf{1}^{+\bullet}) = 9.40 \pm 0.03$ eV agrees with the onset of the overall photoelectron (PE) spectrum (lower inset in Fig. 1). While PE spectra of small, cold neutrals provide precise IE and reflect the Franck–Condon patterns associated with vertical ionization, the thermal energy content of polyatomic samples having room temperature broadens the PE spectra [35]. With respect to the difference between adiabatic and vertical ionization energies ($\Delta IE_{v/a}$), let us therefore first consider the extremes. If $\Delta IE_{v/a}$ is small compared to the internal energy content of the neutral precursor, the resulting PE spectrum shows a sharp rise corresponding to the $0 \rightarrow 0$ transition of the neutral to the cation. If $\Delta IE_{v/a}$ is large, the $0 \rightarrow 0$ transition is unlikely to occur, and the maximum of the PE spectrum occurs for the $0 \rightarrow n$ transition having the best Franck–Condon factor. As rovibrationally excited neutrals also contribute for a polyatomic sample at room temperature, the resulting PE spectra may show smooth, non-characteristic onsets. The PE spectrum of valeramide is in-between the two extremes in that neither a sharp $0 \rightarrow 0$ transition nor a particularly slow rise is observed. Conservatively, we only conclude at this point that $AE(\mathbf{1}^{+\bullet}) = 9.40 \pm 0.03$ eV is an upper bound for IE_a and a lower bound for IE_v. The theoretical treatment (Part II) shall evaluate the margin of these boundaries.

Due to memory effects, only two labeled valeramides were examined with PI methods (see experimental section). Fig. 2 shows PI mass spectra of the [4,4-D_2]-compound **1e** at three selected photon energies. Similar to the unlabeled system, loss of propene already occurs at the PI threshold. Further, consistent with the conclusions derived from the studies using the sector instrument, the elimination of C_3H_5D ($\Delta m = -43$) prevails in the McLafferty reaction, yet some H/D exchange leading to $\Delta m = -44$ is observed as well. With increasing photon energy, the fragmentation via the C_3-route increases while the molecular ion abundance of $\mathbf{1e}^{+\bullet}$ decreases. Again in agreement with the sector data, the KIE associated with the McLafferty rearrangement appears to be small, i.e., the appearance energy of the fragment due to loss of C_3H_5D from **1e** as well as the abundance relative to the parent ion agree with the results for the unlabeled compound within experimental error. As far as the C_2-route is concerned, the results further confirm the mechanistic picture derived so far. Thus, the mass differences of $\Delta m = -29$, -30, and -31 in the PI spectra agree with those observed in the sector instrument. The preference for direct $C_2H_5^\bullet$

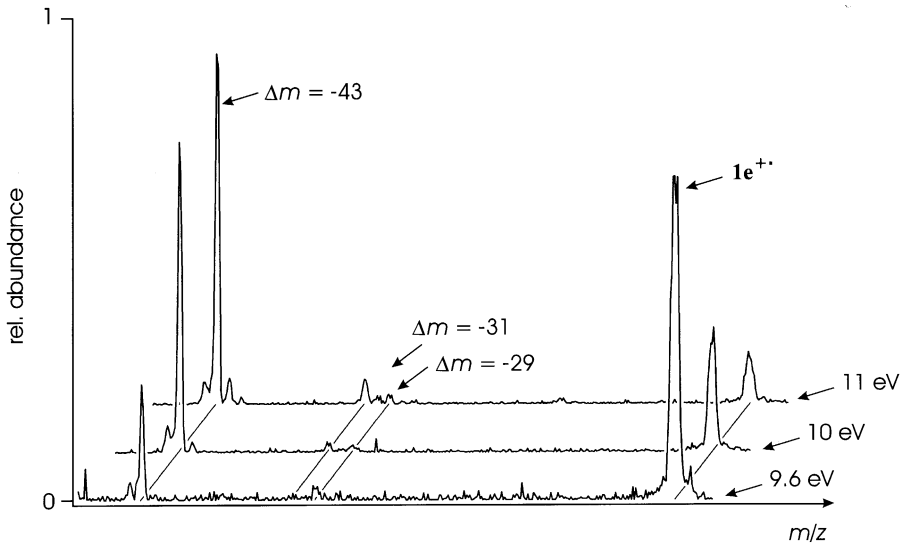

Fig. 2. Photoelectron spectra of [4,4-D_2]-valeramide **1e** at photon energies of 9.6, 10.0, and 11.0 eV, respectively. The small peaks at $\Delta m = -42$ are attributed to natural ^{13}C-isotopes as well as a abstaction of an allylic hydrogen from propene by the enol cation radical $\mathbf{4}^{+\bullet}$ ("McLafferty + 1" fragment)

loss from $\mathbf{1}^{+\bullet}$ at higher photon energies as deduced above, is supported by the increased loss of $C_2H_3D_2^{\bullet}$ ($\Delta m = -31$) at 11 eV. For **1g** (data not shown), the expected loss of $C_3H_2D_4$ ($\Delta m = -46$) prevails in the McLaffety route, while some H/D exchange to $\Delta m = -47$ is observed again. Above 12 eV, the C_2-route is dominated by loss of $C_2D_5^{\bullet}$ ($\Delta m = -34$), i.e., the intact terminal ethyl group. However, we refrain from a more detailed analysis of the isotope distributions in the C_2-route because the corresponding signal-to-noise ratios are much lower than in the sector experiments, primarily not because of the lower sensitivity of the PI experiments, but due to the much less favorable C_3/C_2 branching ratios.

In order to refine the insight into the energetics of the system, unlabeled valeramide was studied by threshold photoelectron-photoion coincidence (TPEPICO) experiments [16,36]. While the resulting breakdown diagram (Fig. 3) is similar to that shown in Fig. 1, the internal energy of the ions is more accurately defined in the coincidence measurements. Specifically, only those ions are detected in which the kinetic energy of the PE is smaller than 50 meV. Hence, the internal energy of the ions is given as: $E_{\mathrm{int}}(\mathbf{1}^{+\bullet}) = h\nu - \mathrm{IE_v}(\mathbf{1}) + \Delta\mathrm{IE_{v/a}}(\mathbf{1}) + E_{298}(\mathbf{1})$, where, $h\nu$ is the photon energy, $\mathrm{IE_v}$ the vertical ionization energy, $\Delta\mathrm{IE_{v/a}}$ the difference between vertical and adiabatic ionization energies, and E_{298} the internal energy of the neutral precursor at room temperature. The major difference of Figs. 1 and 3 is the more rapid decline of the parent in the TPEPICO experiment. Thus, already at 10 eV the molecular ion is almost negligible in Fig. 3, while it persists up to 20 eV in Fig. 1. This effect can easily be attributed to the energy carried away by the PE in the experiments without coincidence and is not pursued any further. Otherwise, the apparent onsets and product distributions agree nicely with those described above. In particular, note that the C_3/C_2 ratio also is large in the TPEPICO data.

In addition to the photon energies, the ion masses, and the energies of the PE, the TPEPICO data obtained with CERISES contain another piece of information which turns out to be quite insightful in the present case. Thus, the velocities of the parent ion and of the fragments formed by dissociative PI in the

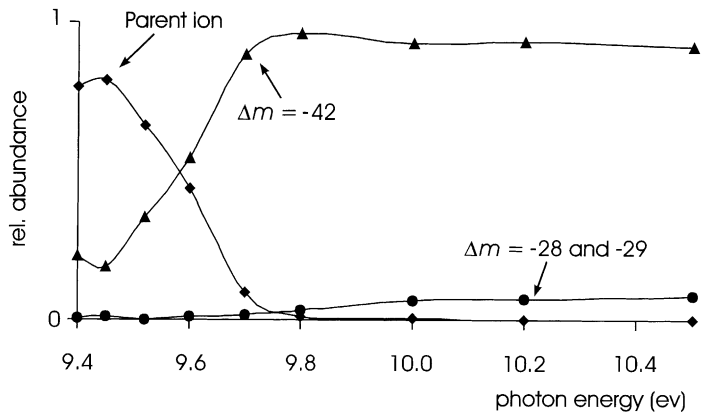

Fig. 3. TPEPICO breakdown diagram for the photoionization of valeramide **1** at different photon energies. Only the parent ion, the C_2- and C_3-channels were monitored. Further, the mass resolution of the quadruple analyzer was lowered such that C_2H_4 and $C_2H_5^{\bullet}$ losses ($\Delta m = -28$ and -29) were not resolved. The diagram is constructed from the experimental data given in Table 4, where the sum of directly and metastably formed fragments is used.

source slightly differ in that the lighter fragments arrive somewhat earlier at the detector than the parent. If, however, the fragments are formed by unimolecular decay of metastable parent ions in the octopole in front of the mass-analysis quadruple, they bear a time-of-flight more closer to that of the parent. Fig. 4 illustrates these features for the TPEPICO experiment conducted at 9.6 eV. Accordingly, the prompt and delayed photofragmentations can be deconvoluted by the related time-of-flight patterns. We note in passing that the TPEPICO study thereby very much mimicks the MI studies conducted in the sector-field mass

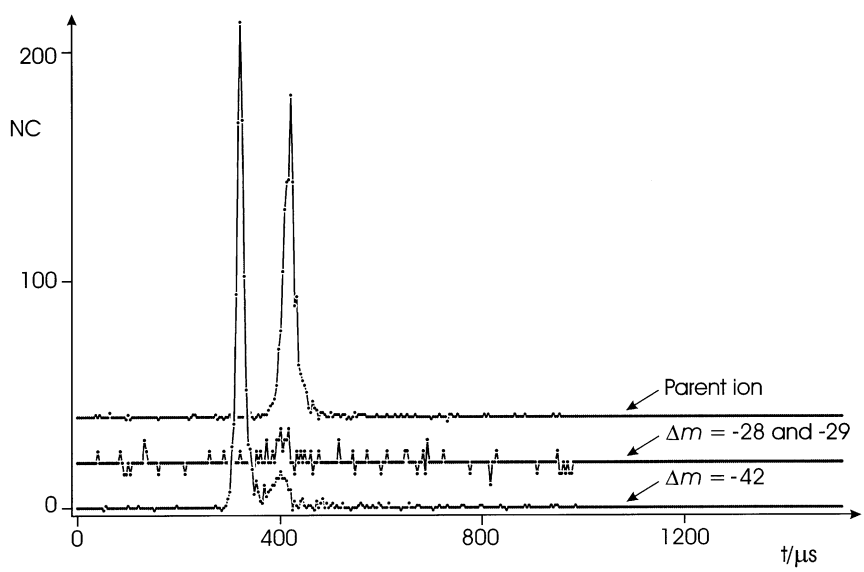

Fig. 4. Time-of-flight distributions of the fragments due to the C_2-route ($\Delta m = -28$ and -29) and the C_3-route ($\Delta m = -42$) as well as of the parent ion $\mathbf{1}^{+\bullet}$ in the TPEPICO experiment conducted at a photon energy of 9.6 eV.

Table 4
Normalized intensities[a] of the parent ion $M^{+\bullet}$ and of the fragments corresponding to the C_2- ($\Delta m = -28$ and -29)[b] and C_3-routes ($\Delta m = -42$) formed directly (**d**), by dissociation of the metastable parent ion within the octopole (**m**), and their sum as derived from the TPEPICO experiments conducted with valeramide at different photon energies

$E(h\nu)$ (eV)	NC[c]	$M^{+\bullet}$	$C_2\mathbf{d}$[b,d]	$C_2\mathbf{m}$[b,d]	ΣC_2[e]	$C_3\mathbf{d}$	$C_3\mathbf{m}$	ΣC_3[e]
9.40	266	78.2	0.0 (0)	0.4 (1)	0.4	18.4	3.0	21.4
9.45[f]	228	80.7	0.4 (1)	0.9 (2)	1.3	13.6	4.4	18.0
9.52	1008	65.2	0.1 (1)	−0.1 (−1)	0.0	29.1	5.7	34.8
9.60	2063	44.4	0.1 (3)	0.9 (18)	1.0	46.8	7.8	54.6
9.70	2388	9.3	0.7 (16)	0.6 (14)	1.3	84.5	4.9	89.4
9.80	2599	1.2	1.3 (33)	1.2 (30)	2.5	92.9	3.4	96.3
10.00[g]	364	0.5	4.9 (18)	1.4 (5)	6.3	91.0	2.2	93.2
10.20	2317	0.0	6.1 (141)	0.7 (16)	6.8	90.4	2.8	93.2
10.50	2153	–[h]	7.8 (167)	0.3 (6)	8.1	91.0	0.9	91.9

[a] Normalized to $\Sigma = 100$. Unless stated otherwise, 6–10 scans were accumulated.
[b] The TPEPICO experiments were performed at low mass resolution of the quadruple analyzer, such that the C_2-channel represents the sum of C_2H_4 and $C_2H_5^\bullet$ losses.
[c] Number of total counts in the TPEPICO spectra provided in order to assess the significance of counting statistics.
[d] Total counts given in brackets. At low counting rates, negative values may arise from the correction for false coincidences.
[e] Sum of directly and metastably generated fragments which is used in Fig. 3.
[f] Two scans only.
[g] Because beam time elapsed, this particular experiment was stopped after two scans.
[h] In order to save beam time, the parent ion was not recorded at this particular photon energy.

spectrometer, while the internal energy of the incident ions formed in the source is controlled much better in the PI study.

In order to analyze this behavior and to acknowledge the experimental uncertainties, the TPEPICO data are to be considered in more detail, because some of them are subject to counting statistics (Table 4). Let us first address the sum of directly and metastably formed photofragments shown in Fig. 3. At ionization threshold, the parent ion predominates, while some of the McLafferty product ($\Delta m = -42$) is already observed. With increasing photon energy, the parent ion intensity rapidly declines and vanishes at 10 eV, concomitant with an increase of $\Delta m = -42$. A significant abundance of the C_2-channel (represented as the sum of $\Delta m = -28$ and -29 in the TPEPICO data) is first seen at 9.6 eV, consistent with the appearance energy of 9.58 ± 0.05 eV derived above. As far as the MI fractions in both channels are concerned, their proportions generally decrease with increasing photon energies, i.e., precisely what is expected for MI dissociation. However, the energy dependence of the corresponding channels does not obey the characteristics of a simple ion dissociation. This aspect is of prime importance and best illustrated by reference to the experiment conducted at 9.6 eV (Fig. 4). At this energy, the parent and the McLafferty product ion show a ca. 1:1 ratio. The C_2-channel is by and large only seen in the metastable fraction, consistent with the photon energy of 9.6 eV being very close to the threshold of this particular fragmentation, such that dissociation via this route can only occur at extended lifetimes of the parent. While the strong competition of the McLafferty channel is obvious in more or less prompt photofragmentation (C_3/C_2 ca. 300) as well as the sum of the prompt and metastable pathways (C_3/C_2 ca. 50), the C_3/C_2 ratio of the MI amounts to only about 10. These differences lead to a fundamental discrepancy, if simple dissociative PI is considered. By definition, the prompt photofragments are formed from ions having larger internal energies than those formed at extended timescales. Irrespective of the nature of the parent ion and the underlying fragmentation mechanisms, the reaction with the lower threshold will therefore predominate the lower the internal energy of the parent. Precisely the opposite is

observed in the TPEPICO experiment at 9.6 eV, in that the C_3/C_2 ratio of the short-lived parent ions is larger than that of the long-lived MI, while the C_2-route seems to bear a higher threshold energy. The same conclusion evolves from the experiments conducted at higher photon energies (Table 4). Consequently, one or several of the underlying assumptions must be incorrect. Specifically, either the C_2- has a lower threshold than the C_3-route, for which we have no indications at all, or not only a single type of parent ion is formed. In fact, the situation can be explained, if the C_2- and C_3-routes are, to some extent, independently accessed upon PI and involve different intermediates which do not readily interconvert into each other. In other words, the TPEPICO results provide an independent confirmation of the proposed uncoupling of the C_2- and C_3-routes derived from the labeling distributions in the sector experiments. With respect to the variations in the C_3/C_2 ratios, it is therefore implied that either MI and PI experiments do not probe the same ion populations and/or the populations of the neutrals precursors differed in both experiments.

4. Conclusions

Sector mass spectrometry and PI experiments provide an internally consistent mechanistic picture for the unimolecular dissociation of ionized valeramide. Thus, γ-C–H bond activation according to the McLafferty rearrangement (C_3-route) predominates, while δ-C–H bond activation (C_2-route) can compete to a notable extent. At elevated energies, also β-C–H bond activation (C_1-route) as well as direct C(3)–C(4) bond cleavage occur. The PI experiments reveal that the C_2- and C_3-routes have rather low thresholds, where occurrence of the latter is observed even at PI threshold. Almost all results, including several subtle mechanistic details, such as the competition of direct and indirect $C_2H_5^{\bullet}$ losses, are consistent with the results obtained in both experimental approaches. Moreover, the labeling distributions can be reproduced reasonably well by a kinetic modeling which explicitly includes the competition of C_2- and C_3-routes. The most interesting result of the modeling is that the KIEs associated with the initial C–H bond activations are surprisingly small. In fact, KIE(γ-C–H) = 1.03 found for the McLafferty route disputes a significant contribution of H(D) migration to the rate-determining step.

Irrespective of the wealth of agreement, the C_3/C_2 ratio, i.e., one of the gross parameters, shows pronounced, seemingly random variations when comparing the different kinds of experiments performed. Far beyond the experimental error margins, the C_3/C_2 ratios range from almost 1 for the MI formed upon EI in the sector instrument to about 4 for the MI in the TPEPICO experiments as well as the 70 eV EI spectrum, ca. 6 in the PI experiments at energies above 10 eV photon energy, and finally exceed 100 at photon energies below 9.6 eV. The mechanistic analysis of both the sector-field experiments and the PI studies suggests that this behavior is associated with the uncoupling of these two routes. Thus, dependent on the precise experimental conditions, both the structures and internal energies distributions of the parent ion(s) may differ. Before addressing these aspects more rigorously, some theoretical insight into the behavior of ionized valeramide is definitely desirable.

Acknowledgements

Financial support by the Deutsche Forschungsgemeinschaft, the Fonds der Chemischen Industrie, the Volkswagen-Stiftung, and the Gesellschaft von Freunden der Technischen Universität Berlin is gratefully acknowledged. We are indebted to C. Alcaraz and the entire staff of LURE, Orsay, for helpful assistance in the PI experiments using synchrotron radiation, and thank A. Chabane and J.-F. Bernadac for their cooperation. D.S. thanks the Laboratoire Chimie-Physique at Orsay for a visiting professorship which formed the basis of this collaboration.

Appendix A. Kinetic modeling of the metastable ion data

In order to avoid numerical errors in the kinetic modeling of the MI data, the ion intensities were

Table 5
Mass differences (Δm in amu), normalized intensities, and branching ratios of C_1-, C_2-, and C_3-channels observed in the corrected MI spectra of $B(1)/E(1)$ mass-selected $\mathbf{1}^{+\bullet}$ and its isotopologs[a,b]

	C_1	−15	−16	−17	−18	−19	C_2	−28	−29	−30	−31	−32	−33	−34	C_3	−42	−43	−44	−45	−46	−47
1	22	20		2	<1		485	68	416						493	491	2				
1a	24	21			1	2	489	72	415	2					487	485	1	1			
1b	20	16		4	<1		452	72	68	123	189				529	525	4	<1			
1c	13	9	<1	1	3		520	49	294	7	170				467	1	70	396			
1d	25	20		3	2		495	2	246	247					480	194	286	<1			
1e	20	17		2	1		535		205	74	255				445	<1	369	76			
1f	26	2		1	23		414	4	<1	147	150	113			560		4	75	481		
1g	31	1		2	28		420		3	70	24	88	141	94	549		1		1	509	38

[a] Normalized to $\Sigma = 1000$.
[b] Also see footnotes of Table 1 in the text.

included with one digit more than given in Table 1 of the text. Table 5 lists these data, where the fragments are normalized to $\Sigma = 1000$.

The following parameters were used in the kinetic modeling of the unimolecular dissociation of valeramide. From the data obtained with **1** and **1a**, the relative rate constants $k(CH_3^{\bullet}) = 20$, $k(NH_3) = 2$, $k(H_2O) = 1$, $k(C_2H_4) = 70$, $k(C_2H_5^{\bullet})_{direct} + k(C_2H_5^{\bullet})_{indirect} = 417$, and $k(C_3H_6) = 490$ with $\Sigma k_i = 1000$ were used as input and were not changed in the subsequent operations. The relationship between direct and indirect $C_2H_5^{\bullet}$ losses from ionized valeramide was defined by the variable $x_{direct} = k(C_2H_5^{\bullet})_{direct}/[k(C_2H_5^{\bullet})_{direct} + k(C_2H_5^{\bullet})_{indirect}]$.

Guided by the proposed mechanistic schemes, the following KIEs were included as variables. KIE(β-CH), KIE(γ-CH), and KIE(δ-CH) express the primary KIEs associated with the initial C–H(D) bond activations in the C_1-, C_3-, and C_2-routes, respectively, and are applied whenever the corresponding positions are deuterated. In the modeling of the partial H/D equilibrations occurring in the course of the C_2- and C_3-routes, KIE(H/D, C_2) and KIE(H/D, C_3) were included, where the former is attributed to 1,4-H(D) migration $\mathbf{5}^{+\bullet} \rightarrow \mathbf{7}^{+\bullet}$ and the latter stands for the behavior of the [*O*-D]-labeled enol in the McLafferty route. Operation of secondary KIEs is included for the C_2- and C_3-routes. In the McLafferty rearrangement, presence of deuterium in the C(4) position is expressed as KIE(γ-CH′) which acknowledges the effect of the second H(D) atom at C(4) on the activation of the other in compounds **1d**, **1e**, and **1g**. The secondary KIEs due to perdeuteration of the methylene groups involved in the subsequent C(2)–C(3) bond cleavages prior to loss of propene is expressed by KIE(C(2), C_3) and KIE(C(3), C_3), respectively, whenever indicated. Likewise, secondary KIEs are assigned to the C(3)–C(4) bond cleavages in the eliminations of C_2H_4 and $C_2H_5^{\bullet}$, i.e., KIE(C(3), C_2H_4), KIE(C(4), C_2H_4), KIE(C(3), $C_2H_5^{\bullet})_{direct}$, KIE(C(4), $C_2H_5^{\bullet})_{direct}$, KIE(C(3), $C_2H_5^{\bullet})_{indirect}$, and finally KIE(C(4), $C_2H_5^{\bullet})_{indirect}$.

Partial H/D exchange processes in the various routes were included by introducing phenomenological parameters x_{scr}, where $x_{scr} = 0$ indicates complete absence of H/D equilibration and $x_{scr} = 1$ stands for statistical H/D distributions between the positions involved. In the McLafferty rearrangement, $x_{scr}(C_3)$ stands for the fraction that undergoes equilibration of the H(D) atoms at C(3) and C(5) with the OH(OD) group of the enol fragment with KIE(H/D, C_3) being operative also (see above). Further, the C(3) and C(5) positions are allowed to participate in different portions in H/D equilibration (see text), as expressed by x_{scr}(C(3)/C(5)). In the indirect loss of ethyl radical, the pair-wise equilibration between C(2)/C(3) and C(4)/C(5) was assumed to be complete; this also results from the modeling when the amount of equilibration is allowed to change. Further, H/D exchange between C(2) and C(5) was described by $x_{scr}(C_2)$, where KIE(H/D, C_2) is operative also (see above). In the C_1-route, a 10:1 ratio of specific and

Table 6
Modeled intensities and branching ratios of C_1-, C_2-, and C_3-channels for $\mathbf{1}^{+\bullet}$ and its isotopologs where the deviations from the data in Table 5 are given behind the dashes[a,b]

	C_1	−15	−17	−18	−19	C_2	−28	−29	−30	−31	−32	−33	−34	C_3	−42	−43	−44	−45	−46	−47
1	23/+1	20/±0	2/±0	1/+1		487/+2	70/+2	417/±1						491/−2	491/±0	–[d]/−2				
1a	23/−1	20/−1		1/±0	2/±0	487/−2	70/−2	417/+2	–[c]/−2					490/+4	490/+5	–[c]/−1	–[c]/−1			
1b	25/+6	20/+4	4/±0	1/+1		451/−1	78/+6	89/+21	113/−10	171/−18				523/−6	523/−2	–[c,d]/−4				
1c	18/+5	15/+6	–[c]/−1	3/±0		515/−5	52/+3	272/−22	–[c]/−7	191/+21				467/+1	–h/−1	71/+1	396/±0			
1d	25/+0	22/+2	2/−1	1/−1		494/−1	–[c]/−2	256/+10	238/−9					481/+1	189/−5	292/+6	–[c]/±0			
1e	27/+7	24/+7	2/±0	1/±0		508/−27		204/−1	69/−5	235/−20				465/+20	–[c]/±0	386/+15	79/+3			
1f	26/±0	2/±0	2/+1	22/−1		396/−18	–[c]/−4	–[c]/±0	152/+5	151/+1	93/−20			577/+17		–[c,d]/−4	74/−1	503/+22		
1g	33/+2	3/+2	3/+1	27/−1		428/+9		–[c]/−3	72/+2	17/−7	94/+6	145/+4	100/+6	540/−9		–[c,d]/−1		–[c]/−1	497/−12	42/+4

[a] Normalized to $\Sigma = 1000$.

[b] The average deviation is ±4; the largest deviations of about 20 occur in the C_2 channels of **1b**, **1c**, **1e**, and **1f** ($\Delta m = -29$ to -32) and in the McLafferty route for **1f** ($\Delta m = -45$).

[c] Losses of isotopically scrambled fragments are not included in the modeling.

[d] Elimination of $\Delta m = -43$ amu is not included in the modeling.

Table 7
Optimized parameters used in the kinetic modeling leading to the data given in Table 6, their lower and upper bounds derived from the sensitivity analysis,[a] and the values used in the simplified model mentioned used for Table 2 of the text

	Optimized	Lower bound	Upper bound	Δ_{max} (%)[b]	Sensitivity	Simple model[c]
x_{direct}	0.19	0.17	0.21	10	+	0.18
KIE(β-CH)	1.6	1.3	8[d]	8[d]	–[d]	1.7
KIE(γ-CH)	1.03	0.97	1.11	5	+	1.01
KIE(δ-CH)	1.32	1.17	1.38	10	+	1.30
KIE(H/D, C_2)	2.0	1.4	2.6	30	+/–	1.8
KIE(H/D, C_3)	1.9	1.5	3.3	70	–	1.9
KIE(γ-CH′)	1.07	1.01	1.17	9	+	–[e]
KIE(C(2), C_3)	1.05	0.93	1.15	10	+	–[e]
KIE(C(3), C_3)	1.19	1.13	1.30	9	+	1.12
KIE(C(3), C_2H_4)	1.53	1.0	4.5	200	–	–[e]
KIE(C(4), C_2H_4)	1.23	0.85	3.5	200	–	–[e]
KIE(C(3), $C_2H_5^{\bullet}$)$_{direct}$	1.11	0.87	1.27	10	+	–[e]
KIE(C(4), $C_2H_5^{\bullet}$)$_{direct}$	1.6	0.93	3.0	90	–	–[e]
KIE(C(3), $C_2H_5^{\bullet}$)$_{indirect}$	1.00	0.94	1.09	9	+	–[e]
KIE(C(4), $C_2H_5^{\bullet}$)$_{indirect}$	1.01	0.88	1.08	10	+	–[e]
$x_{scr}(C_2)$	0.19	0.05	0.32	70	–	0.16
$x_{scr}(C_3)$	0.28	0.26	0.34	20	+/–	0.28
x_{scr}(C(3)/C(5))	0.54	0.36	0.58	30	+/–	0.54

[a] Acceptance thresholds are maximal deviations of ±30 for the separate channels of the C_2- and C_3-routes and ±10 for the separate channels of the C_1-route; see text of Appendix A.
[b] Largest deviation in percent (rounded to one significant digit).
[c] After re-optimization.
[d] Not reached for these threshold conditions.
[e] Parameter omitted in the simple model.

non-specific $CH_3^{\bullet}$ losses was assumed and not optimized any further. Based on experiment, equilibration was neglected for the direct losses of ethene and ethyl radical in the C_2-route. For the minor eliminations of ammonia and water KIEs were neglected entirely.

Optimization of all parameters using least square criteria applied to the overall and the relative deviations while acknowledging the boundary conditions as defined in the text, leads to the modeled intensities given in Table 6; the optimized parameters are given in Table 7. The agreement between the measured and the modeled intensities is reasonable in general, and within the experimental error margins in particular. The average deviation amounts to ±4; maximal deviations (ca. ±20) occur for $\Delta m = -29$ and -31 from **1b** and **1c**, $\Delta m = -31$ from **1e**, and $\Delta m = -31$ and -45 from **1f**.

The resulting scheme of equations is quite complex, and linear dependencies cannot be excluded. Therefore, some kind of sensitivity analysis is essential in order to evaluate the significance of the different variables. For this purpose, maximal deviations of ±30 were applied to the separate channels of the C_2- and C_3-routes as well as the overall branching ratios, while only ±10 was allowed in the C_1-route. These margins were then considered as acceptance thresholds. Further, because the sensitivity of the parameters must not be equal upon in- or decrease, the upper and lower bounds for reaching the acceptance thresholds are given in Table 7 together with the maximal deviations Δ_{max} in percent. The latter are also used for the qualitative evaluation of the sensitivity of the various parameters as large (+), medium (+/–), or small (–).

As a result of the sensitivity analysis and in order to probe the robustness of the modeling, it was attempted to ignore all secondary KIEs while re-optimizing the remaining parameters and simultaneously increasing the acceptance thresholds of the C_2- and C_3-routes

to ±40. This simplified approach was possible for all parameters mentioned above, except of KIE(C(3), C_3) operative in the McLafferty rearrangement. For KIE(C(3), C_3) = 1.0, the experimentally observed decrease of the McLafferty route for compound **1c** is not reproduced and results in a severe underestimation of the C_2-channel. Otherwise, the differences between the more complex model discussed above and the more simple one are acceptable. Further, also the optimized variables agree pretty well. Therefore, only the simplified model is presented in Table 2. In the text, however, the values from the more complex model are used because the associated sensitivity analysis also allows for error estimates.

References

[1] F.W. McLafferty, Anal. Chem. 28 (1956) 306.
[2] F.W. McLafferty, Anal. Chem. 31 (1959) 82.
[3] D. Kingston, J. Bursey, M. Bursey, Chem. Rev. 74 (1974) 223.
[4] R. Weber, K. Levsen, C. Wesdemiotis, T. Weiske, H. Schwarz, Int. J. Mass Spectrom. Ion Phys. 43 (1982) 131.
[5] H. Schwarz, T. Weiske, K. Levsen, A. Maquestiau, R. Flammang, Int. J. Mass Spectrom. Ion Phys. 45 (1982) 367.
[6] T. Weiske, H. Schwarz, Chem. Ber. 116 (1983) 323.
[7] T. Weiske, H. Halim, H. Schwarz, Chem. Ber. 118 (1985) 495.
[8] D.J. Harvey, Org. Mass Spectrom. 28 (1993) 287.
[9] M. Takayama, Int. J. Mass Spectrom. Ion Processes 144 (1995) 199.
[10] D. Kreft, H.F. Grützmacher, Eur. J. Mass Spectrom. 4 (1998) 63.
[11] J. Loos, Diplomarbeit, TU Berlin, 2000.
[12] C.A. Schalley, D. Schröder, H. Schwarz, Int. J. Mass Spectrom. Ion Processes 153 (1996) 173.
[13] K.L. Busch, G.L. Glish, S.A. McLuckey, Mass Spectrometry/Mass Spectrometry: Techniques and Applications of Tandem Mass Spectrometry, VCH, Weinheim, 1988.
[14] D. Schröder, H. Schwarz, Int. J. Mass Spectrom. Ion Processes 146/147 (1995) 183.
[15] O. Dutuit, C. Alcaraz, D. Gerlich, P.M. Guyon, J.W. Hepburn, C. Metayer-Zeitoun, J.B. Ozenne, T. Weng, Chem. Phys. 209 (1996) 177.
[16] T. Baer, in: M.T. Bowers (Ed.), Gas Phase Ion Chemistry, Academic Press, New York, Vol. 1, 1979, p. 153.
[17] D. Schröder, W. Zummack, H. Schwarz, J. Am. Chem. Soc. 116 (1994) 5857.
[18] Y. Horiguchi, S. Matsuzawa, E. Nakamura, I. Kuwajima, Tetrahedron Lett. 27 (1986) 4025.
[19] NIST Chemistry WebBook, http://webbook.nist.gov/.
[20] M. Abebe, A. Maccoll, R.D. Bowen, Eur. Mass Spectrom. 3 (1997) 197.
[21] K.M. Stirk, L.K.M. Kiminkinen, H.I. Kenttämaa, Chem. Rev. 92 (1992) 1649.
[22] H.I. Kenttämaa, Org. Mass Spectrom. 29 (1994) 1.
[23] P. Mourgues, C. Monteiro, H.E. Audier, S. Hammerum, Org. Mass Spectrom. 25 (1990) 389.
[24] C. Trage, W. Zummack, D. Schröder, H. Schwarz, Angew. Chem. Int. Ed. 40 (2001) 2708.
[25] M.B. Stringer, D.J. Underwood, J.H. Bowie, C.E. Allison, K.F. Donchi, P.J. Derrick, Org. Mass Spectrom. 27 (1992) 270.
[26] J.M.H. Pakarinen, P. Vainiotalo, C.L. Stumpf, D.T. Leeck, P.K. Chou, H.I. Kenttämaa, J. Am. Soc. Mass Spectrom. 7 (1996) 482.
[27] C.K. Lin, S.Y. Chen, M.H. Lien, J. Phys. Chem. 99 (1995) 1454.
[28] H. Schwarz, Org. Mass Spectrom. 15 (1980) 491.
[29] H. Schwarz, Top. Curr. Chem. 97 (1981) 1.
[30] A. Thibblin, P. Ahlberg, Chem. Soc. Rev. 18 (1989) 209.
[31] T. Weiske, H. Schwarz, Tetrahedron 42 (1986) 6245.
[32] P. Mourgues, J. Chamot-Rooke, H. Nedev, H.-E. Audier, J. Mass Spectrom. 36 (2001) 102.
[33] T. Drewello, N. Heinrich, W.P.M. Maas, N.M.M. Nibbering, T. Weiske, H. Schwarz, J. Am. Chem. Soc. 109 (1987) 4810.
[34] E.P.L. Hunter, S.G. Lias, J. Phys. Chem. Ref. Data 27 (1998) 413.
[35] K.M. Ervin, Chem. Rev. 101 (2001) 391, and references therein.
[36] J. Riley, T. Baer, J. Phys. Chem. 97 (1993) 385.